Peer-reviewed version available at *Electronics* **2019**, *8*, 1351; doi:10.3390/electronics8111351

Article

Effects of the Body Wearable Sensor Position on the UWB Localization Accuracy

Timothy Otim [1]*, Luis E. Díez [1], Alfonso Bahillo [1], Peio Lopez-Iturri [2], and Francisco Falcone [2]

[1] Faculty of Engineering, University of Deusto, Av. Universidades, 24, 48007, Bilbao, Spain; {otim.timothy, luis.enrique.diez, alfonso.bahillo}@deusto.es.

[2] Department of Electric, Electronic and Communication Engineering and Institute for Smart Cities, Public University of Navarra, 31006, Pamplona, Spain; {peio.lopez, francisco.falcone} @unavarra.es

* Correspondence: otim.timothy@deusto.es

Abstract: In recent years, several Ultrawideband (UWB) localization systems have already been proposed and evaluated for accurate position estimation of pedestrians. However, most of them are evaluated for a particular wearable sensor position; hence the accuracy obtained is subject to a given wearable sensor position. In this paper, we study the effects of body wearable sensor positions i.e., chest, arm, ankle, wrist, thigh, fore-head, hand, on the localization accuracy. The conclusion drawn is that the fore-head is the best, and the chest is the worst body sensor location for tracking a pedestrian. While the fore-head position is able to set an error lower than 0.35 m (90th percentile), the chest is able to set 4 m. The reason for such a contrast in the performance lies in the fact that in NLOS situations, the chest as an obstacle is larger in size and thickness than any other part of the human body, which the UWB signal needs to overcome to reach the target wearable sensor. And so, the large errors arise due to the signal arriving at the target wearable sensor from reflections of a nearby object or a wall in the environment.

Keywords: Ultrawideband (UWB); Localization; Ranging; Body wearable sensors; Human body shadowing

1. Introduction

Wearable technology holds a great deal of promise, therefore in 2025 its market is expected to reach $ 70 billion [1]. Wearables are capable of delivering unprecedented opportunities for tackling societal challenges by providing solutions in the areas of healthy ageing, patient monitoring, emergency management, safety at work, productivity enhancement and others. Therefore, major sectors in this market are expected to remain as consumer electronics, defence, and healthcare. Usually, the market sector that the wearable aims to address often determines its position on the body. For instance, in emerging opportunities for localization and tracking, wearables can be positioned at the ankle, head, and wrist for monitoring of inmates in prisons, miners trapped in mines and patients inside hospitals, respectively [2]. A key application and one of the most relevant nowadays of wearables in any sector is in localization and navigation systems [3–5]. Infact, nowadays wearables can include for instance (i) inertial sensors for measuring the angular velocity and linear acceleration, (ii) magnetometer for measuring the heading, (iii) proximity sensors for detecting if a defined subject or obstacle is present nearby.

Estimation of the position of a target in an outdoor environment is performed using Global Navigation Satellite Systems (GNSS) such as Global Positioning Systems (GPS). In the case of indoor environments, GNSS can not work properly due to poor coverage of satellite signal [6–9]. For this reason, research efforts in the field of positioning have been directed towards indoor scenarios with an aim of establishing a standard indoor positioning system (IPS) that can be applied worldwide.

In indoor areas, a large category of traditional positioning technologies is beacon based–where pre-installed infrastructure at known positions are used to transmit signals whose measurements of

received strength, time of flight (TOF), and angle of arrival are used in estimating the position of a moving object. Nonetheless, this kind of localization technique is still an open problem because of the inability to adequately overcome the combined effects of pathloss, multipath fading, and human body shadowing. Many different approaches have been proposed to obtain a similar performance to the GNSS outdoors [10]. For instance, Wi-Fi, Ultrawideband (UWB), or Ultrasound, and advanced processing techniques, such as Kalman and Particle Filters, have been proposed to cope with the deterioration in performance due to combined effects of pathloss and multipath fading. Among the most accurate beacon-based localization solutions are those that rely on ultrasound or UWB radio signals [11]. Thanks to properties, such as ability to have decimeter-level location estimates, immunity to fading, low-power transmission, and low-cost implementation, UWB technology has gained a lot of interest in the academic and industry research. In fact according to [12], Apple is considering the use of UWB radio technology for a future version of iBeacon for precision tracking as well as including an UWB interface in the new iPhone 11.

Though in recent years, there has been a great deal of interest in the use of UWB for ranging and positioning [13–15], its performances deteriorate in non-line-of sight (NLOS). In tracking context of pedestrians using UWB technology, an important factor which has been often overlooked but has significant effect on the ranging and positioning error is the influence caused by the human body itself in NLOS situations. The effects of human body shadowing are additional propagation losses or biases in TOF measurements when the body blocks the line-of-sight (LOS) between a wearable sensor and an anchor. These effects, which generally depend on: i) body wearable sensor position and ii) relative heading angle (RHA), are currently not adequately accounted for and will decrease the accuracy of localization systems. The error caused by human body shadowing is in many cases so important as the range errors caused by infrastructure obstruction as errors of several meters can be detected. In fact, the human body is the only obstacle for sure will be always present regardless the environment.

Currently, studies available on the impact of human body on the positioning error are performed for a particular body wearable position. Additionally, the studies are performed in a static context with discrete angles between the facing direction of the pedestrian and the direction of the body wearable sensor-anchor line. For instance, in [16–18], the authors study the effect of human body obstruction on the ranging and positioning error for the wrist, chest and hand body wearable sensor positions, respectively. In [19], the authors use the Finite Difference Time Domain (FDTD) and empirical techniques to explore human body and UWB radiation interaction on TOF ranging for the hand body location.

A preliminary work has already studied the impact of body wearable sensor positions on UWB ranging [20]; however, the localization aspect was not included in the analysis. Therefore, to the best of our knowledge, there is no work in the literature that studies the impact of human body shadowing on the positioning accuracy when the wearable sensor is at different body locations. In this paper, we present a novel analysis of the effects of the body wearable sensor positions on the UWB localization accuracy. Similar to [20], we perform experiments considering seven body wearable sensor locations namely, fore-head, hand, chest, wrist, arm, thigh and ankle. The aforementioned body wearable positions are chosen because they are the most popular in the market according to Vandrico database [21]. Additionally, the localization performance for the considered body positions is analyzed using an Extended Kalman Filter (EKF).

The rest of this paper is organized as follows: Section II, describes UWB communications in the presence of the human body; the experimental setup and the method adopted to collect the experimental data is described in Section III. The UWB ranging and positioning performance is analyzed in sections IV and V for different body wearable sensor positions. In section VI, the presentation and discussion of results is made. Finally, in the last section, we give some conclusions and future work.

2. The presence of the human body in UWB communications

In the presence of the human body, UWB is capable of correctly measuring the LOS time of arrival. However, when the direct path is blocked by the human body, the NLOS effect creates longer paths which correspond to significant errors from a few decimeters to several meters depending on the position of the wearable sensor on the body. In this section, we describe how the body regions, thorax, limb, and head, influence the ranging error in NLOS situations.

Ideally, when electromagnetic waves interact with the body, part of the signal is reflected, diffracted and the other part is transmitted through the body. Given that the body is composed of various organs with different tissue types [see – Table 1], several electrical characteristics such as relative permittivity, power absorption, conductivity, and path loss are vastly inhomogeneous [22,23]. It is also apparent from Table 1 that these tissues also vary in thickness.

Table 1. Tissue thickness in millimetres for different body regions [24,25]. Note that tissues which are only specific to a body region such as lungs and heart for the thorax, as well as brain and cerebrospinal fluids for the head, have not been included.

Tissue	Thorax	Limbs	Head
Skin	1.4 - 2.6	0.6 - 2.0	0.5 - 2
Fat	0.6 - 15.0	0.4 - 20.6	1 - 2
Muscle	0.0 - 30.0	0.0 - 3.0	0 - 4
Bone	5.6 - 6.6	-	1 - 10

A pulse that is sent towards a target sensor at a given body region (position) will cross several layers, generating attenuation and delay due to the impedance mismatch between adjacent tissues. The additional range error is often proportional to the tissues' relative permittivity and thickness, and can be as important as the range error created by any other obstacle in the environment. In fact, according to [23], this range error is from 0.2 to 0.5 m since RF propagation through the body takes between 0.7 and 1.6 ns. However, the aforementioned range errors are likely to change because UWB propagation between the wearable sensor and anchor combines several characteristics such as LOS, creeping wave, multiple reflections from surrounding environments, and diffraction around a particular body position, which is critical for any robust localization system.

3. Experimental Setup

In this section, we perform experiments to study the effects of the body wearable sensor positions on the UWB ranging and localization accuracy. Throughout this paper, several TREK1000 development kits manufactured by Decawave were used. According to [26] and [11], TREK1000 development kits are the best UWB commercial products for ranging. The nodes are fully compliant with the IEEE 802.15.4-2011 UWB standard and make it possible to achieve ranging measurements using two-way ranging measurements at a rate of 3.57 Hz. For the purpose of these measurement campaigns, one TREK1000 node was configured as a wearable sensor and four nodes were configured as anchors and installed at fixed positions in the Lab. The nodes were made to work with a 110 kb/s data rate and in the channel 2 (3990 MHz).

The experiments were carried out inside the Luis Mercader Lab at the department of Electric, Electronic and Communication engineering at the Public University of Navarra in Spain [see – Fig. 1]. The Lab had the following dimensions: 6 m wide, 13 m long, and 4 m high, and contained a number of computers, monitors, chairs, desks, closets and working people. The floor and ceiling were made of concrete. The floor plan of Lab environment where the tests were performed is showed in Fig. 2.

The floor plan shows detailed anchor positions and a path with 26 ground-truth points with each point approximately 1 m from the other. The coordinates of the tripods and ground-truth marks were measured using a laser rangefinder. The environment did consist of several interfering objects such as pieces of furniture, metallic cabinets and desktop computers. The origin of the reference system was

Preprints (www.preprints.org) | NOT PEER-REVIEWED | Posted: 23 September 2019 doi:10.20944/preprints201909.0266.v1

Peer-reviewed version available at Electronics 2019, 8, 1351; doi:10.3390/electronics8111351

(a) (b)

Figure 1. Details of the Luis Mercader Lab environment. Dimensions: 13 m × 6 m × 4 m. The Lab contains computers, monitors, chairs, desks, and closets which contribute in creating multipath components.

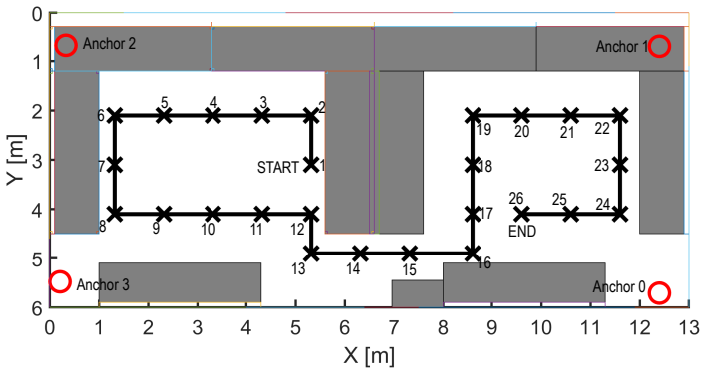

Figure 2. Map of the room and the installation in Luis Mercader Lab. A path with 26 ground-truth points (marked with crosses) was selected. Also shown are the 4 anchors at the corners of the Lab.

Table 2. Coordinates of UWB Anchors, where n is the anchor identity number defined as $n = 0, 1, 2, 3$

Anchor (n)	X (cm)	Y (cm)	Z (cm)
Anchor 0	1240	571	170
Anchor 1	1240	70	173
Anchor 2	548	33	172
Anchor 3	68	21	172

(a) Chest **(b)** Arm **(c)** Ankle **(d)** Wrist **(e)** Thigh **(f)** Fore-head **(g)** Hand

Figure 3. Wearable sensors mounted at different positions on the body. At the hand, the sensor is about 20 cm from the chest since this is a usual place for texting or looking at the screen of a smart phone when locating your position in a real world scenario.

Preprints (www.preprints.org) | NOT PEER-REVIEWED | Posted: 23 September 2019 doi:10.20944/preprints201909.0266.v1

Peer-reviewed version available at Electronics 2019, 8, 1351; doi:10.3390/electronics8111351

defined at the top left corner. The UWB anchors were mounted on tripods in the positions indicated in Table 2.

A male subject, 1.80 m height and 77 kg mass was considered for the measurements. The wearable sensors were mounted on the subject with the help of velcro straps at the right-ankle, right-thigh, fore-head, right-hand, right-arm, chest, and right- wrist as seen in Fig. 3.The heights at which the wearable sensors were mounted are showed in Table 3.

Table 3. Height (H) in centimetres at which the wearable sensors are mounted

	Ankle	Thigh	Fore-head	Hand	Arm	Chest	Wrist
H	15	70	177	120	130	130	90

Using the installed ground-truth marks, firstly, the wearable sensor was mounted on a tripod at a height of 177 cm and moved along the path starting from ground-truth point 1 and ending at ground-truth point 26 [see – Fig. 2] as a reference for further comparisons. Then, for each wearable sensor position, the subject was made to walk the same path following two scenarios (discrete and continuous). In the discrete scenario, the ranges were recorded only when the subject moved to the correct ground-truth point for a period of 30s.

Similar to the work in [26], in the continuous scenario, the ranges were recorded continuously without stopping as the subject moved from the start to end. At each ground-truth point, the subject stood still for approximately 10 s before moving to the next. We repeated the experiment by each body sensor location (7 times) aiming at minimizing any possible interference that could arise among the sensors.

4. Analysis of the ranging performance

The distance between the wearable sensor and the anchors is determined when the TOF and the speed of radio wave propagation are known. Using the test setup described above, we compute the range by measuring the two-way TOF between the wearable sensor and the anchors, and using the speed of light as the speed of the radio waves.

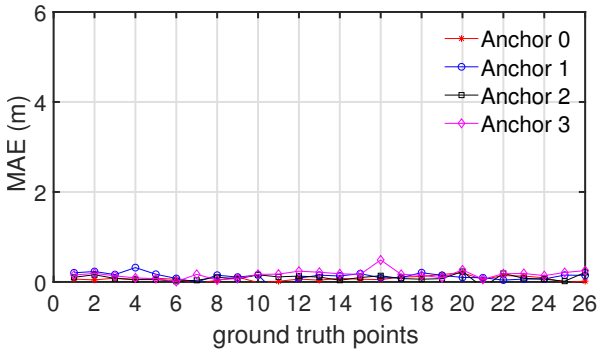

Figure 4. Ranging error without the influence of the human body presence.

In Fig. 4 and Fig. 5, we show the measured error which is computed as the difference between the measured distance and the true distance. Since the measurements were recorded for a period of 30 s, the mean average error (MAE) at a single ground-truth position is generated from at least 100 distance readings. Note that in analyzing the ranging performance, the only ranges from the discrete scenario are used.

Using the measurements taken without the human body presence, we show in Fig. 4, the ranging errors obtained in ideal situations where there is complete LOS. We can appreciate in this figure that the UWB range errors are decimeter-level. In fact, we computed a mean error of 11 cm, and a standard deviation (SD) of 6 cm, which are likely due to multipath.

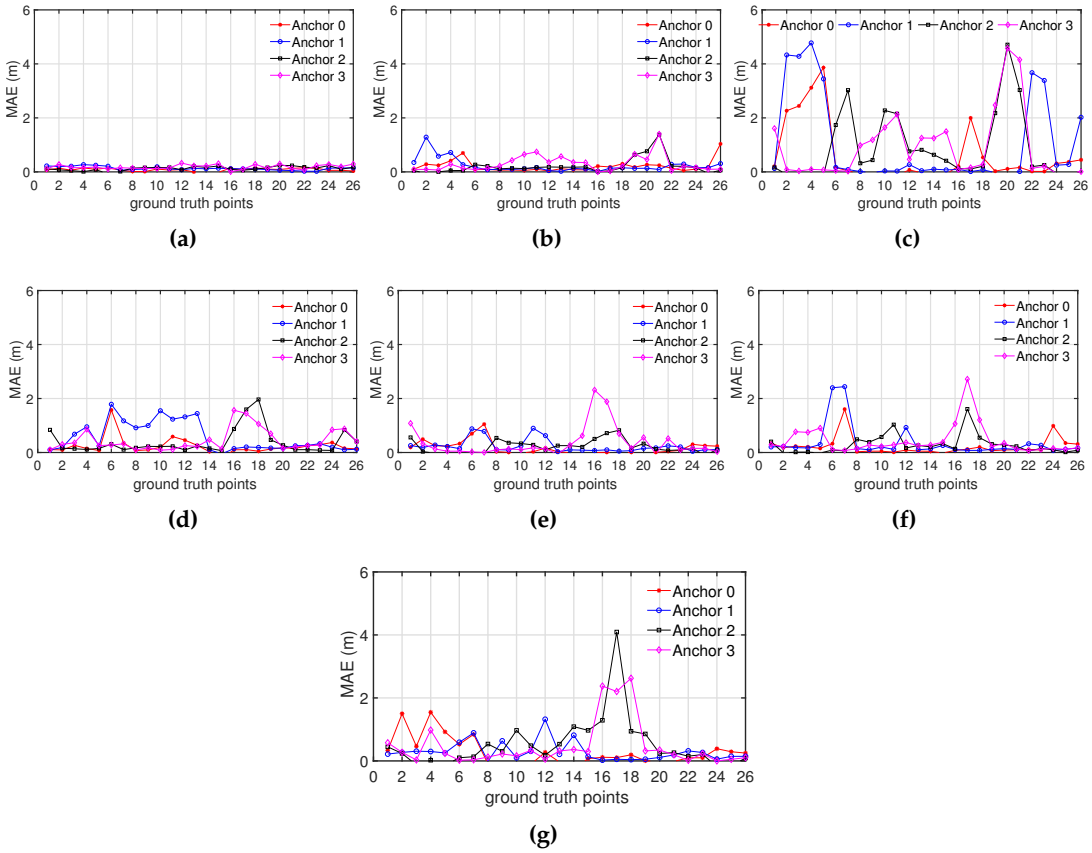

Figure 5. Impact of body wearable sensor positions on the ranging error for: (a) fore-head, (b) hand, (c) chest, (d) ankle, (e) wrist, (f) arm, and (g) thigh.

Looking at Fig. 5, a clear observation is that the range error highly depends on the position where the wearable sensor is placed on the body. In Fig. 5a, we observe that the range error is very stable for the fore-head position. Additionally, low mean range errors of less than 20 cm are observed across all anchors. A possible reason for such a good performance lies in the fact that diffraction, and not direct transmission or even surface waves are the dominant propagation mechanism on the human head [27]. Thus in NLOS, the UWB waves are able to move into the shadow zone, with an increased path length of about 20 cm corresponding to the distance between the back-head and fore-head.

In Fig. 5(b-g), we observe that the range error is highly unstable. The peaks observed correspond to large range errors obtained when the wearable sensor is lying in NLOS conditions with respect to the anchor. Looking at Fig. 5, we see that except for the fore-head, the hand provides a better performance than the rest of the wearable sensor positions. In NLOS, UWB wave propagates to the wearable sensor by creeping wave propagation [28], which is enabled by the space of 20 cm from the chest [see – Fig. 3g].

Similar to the torso, In Fig. 5c, we observe that the chest position provides the worst ranging performance as errors of up to 4.5 m can be observed.The reason is that under NLOS the chest which is part of the torso generates a big shadow zone so the signal cannot reach the sensor by LOS or creeping wave propagation but by any reflection from the surroundings.

In Fig. 5(d-g), we observe that the limbs generate a shadow zone similar to the torso under NLOS. However, the limbs have a lower shadow zone because the limbs are less thicker than the torso. Consequently, the range errors are lower [29]. Additionally, the small differences in the range errors among ankle, ankle, arm, wrist, and thigh in NLOS can be attributed to the differences in the thickness of the limb on which the sensor is attached. i.e., the order of performance is such that the wrist and ankle have almost a similar performance, which is followed by the thigh and arm.

5. Analysing of the positioning performance

Because the main application of ranging is positioning, in this section we compare the positioning performance. As explained in the previous section, the infrastructure of the experiments consists of one UWB node mounted on seven body locations and four UWB nodes in fixed and known positions acting as anchors. In order to achieve the positioning performance, a localization algorithm based on the EKF is implemented. We use range measurements from the continuous scenario. To minimise the adverse effects of NLOS, the measured range errors greater than 2.5 m were rejected in the update of the state vector estimation.

Similar to [30] and [31], the EKF will consist of a discrete time white noise acceleration driven model as the dynamic model and the ranges between the wearable sensor at different body locations and the anchors as the measurements. The dynamic model is modeled as a constant position model driven by acceleration noise instead of a constant velocity model. The position model driven by acceleration noise is equivalent to having a constant velocity = 0. We chose this model because the subject was still most of the time.

The state vector $\boldsymbol{x}_k$ is defined by the 3-D position ($\boldsymbol{p}$) and velocity ($\boldsymbol{v}$) estimates as indicated in (1) as :

$$\boldsymbol{x}_{k|k} = \boldsymbol{x}_k = (\boldsymbol{p}_k \; \boldsymbol{v}_k)^T \tag{1}$$

Therefore, $\boldsymbol{x}_k$ is defined as :

$$\boldsymbol{x}_{k|k-1} = \boldsymbol{F}_k \boldsymbol{x}_{k-1|k-1} + \boldsymbol{w}_k \tag{2}$$

where $\boldsymbol{F}_k$ is the state transition matrix given as :

$$\boldsymbol{F}_k = \begin{pmatrix} 1 & 0 & 0 \\ 0 & 1 & 0 \\ 0 & 0 & 1 \end{pmatrix} \tag{3}$$

Preprints (www.preprints.org) | NOT PEER-REVIEWED | Posted: 23 September 2019 doi:10.20944/preprints201909.0266.v1

Peer-reviewed version available at Electronics 2019, 8, 1351; doi:10.3390/electronics8111351

$\boldsymbol{w}_k$ is the process noise, modeled as a white noise acceleration with covariance matrix $\boldsymbol{Q}_k$:

$$\boldsymbol{Q}_k = \begin{pmatrix} \sigma_{ax}^2 \Delta T^2/2 & 0 & 0 \\ 0 & \sigma_{ay}^2 \Delta T^2/2 & 0 \\ 0 & 0 & \sigma_{az}^2 \Delta T^2/2 \end{pmatrix} \tag{4}$$

where ΔT is equal to the time difference between timestamps $\boldsymbol{k}$ and $\boldsymbol{k}-1$ and $\sigma_{ax} = 100$ cm, $\sigma_{ay} = 100$ cm , and $\sigma_{az} = 10$ cm are the uncertainty that model the acceleration driving noise of the dynamic model in the x, y, and z directions. The state vector $\boldsymbol{x}_k$ is initialized with the coordinates of the first ground-truth point. Their initial standard deviations were set to 20 cm for the x and y coordinates, and 0.5 cm for the z coordinate. Note that, we use a lower uncertainty in the vertical axis than in the horizontal plane because the height at which wearable sensor is located on the body is fixed.

The measurement model has the form:

$$\boldsymbol{z}_k = \boldsymbol{h}(\boldsymbol{x}_{k|k}) + \boldsymbol{n}_k \tag{5}$$

where $\boldsymbol{z}_k$ is the measurements vector, $\boldsymbol{h}$ is the measurement non-linear function, and $\boldsymbol{n}_k$ is the measurement noise with covariance matrix $\boldsymbol{R}_k$.

The SD of the measurement model was set according to Table 4. The values were obtained from a set of measurements to characterize the UWB nodes for each wearable sensor position.

Table 4. The uncertainty in centimetres of the measurement model for each wearable sensor position

	Ankle	Thigh	Fore-head	Hand	Arm	Chest	Wrist
SD	50	60	10	30	50	130	20

Using UWB ranges from the 4 anchors to update the estimate of the state $\boldsymbol{x}_{k|k}$, the measurements take on the following form:

$$z_{n,k} = h_n(\boldsymbol{x}_{k|k}) = \\ = \sqrt{(p_x - a_{x,n})^2 + (p_y - a_{y,n})^2 + (p_z - a_{z,n})^2} \tag{6}$$

where $z_{n,k}$ is the measured range between the nth anchor at the position $a_{x,n}$, $a_{y,n}$, $a_{z,n}$, and wearable sensor with current position estimates at p_x, p_y and p_z.

Because the output of the EKF filter provides a continuous estimation of the position like in Fig. 6, it is necessary to detect when the subject feet are still so that the ground-truth positions are estimated. Therefore, we performed the following tasks

1. Smoothing: where a moving average filter is applied to each position component. The length of the window was empirically set to 4 s.
2. Filtering: in order to reduce the number of outliers in the position estimation, a moving variance with window length of 4 s was also set.
3. To determine the ground-truth position, the *k-means* clustering is applied to the filtered estimates. The ground-truth positions are extorted from the obtained centroids.

An example of the whole process of obtaining the ground-truth positions from the continuous position estimation is shown in Fig. 6 and Fig. 7a for the fore-head position. This procedure was repeated for each of the body wearable positions. And so, the estimated ground-truth points are illustrated in Fig. 7 for the fore-head, hand, arm, and chest locations.

6. Results and Discussion

Using the absolute value of the difference between the real ground-truth positions and the values estimated by the EKF-based localization algorithm as the error metric, in this section, we compare the performance of the wearable body sensor positions with the performance of the tripod, which is

Preprints (www.preprints.org) | NOT PEER-REVIEWED | Posted: 23 September 2019 doi:10.20944/preprints201909.0266.v1

Peer-reviewed version available at Electronics 2019, 8, 1351; doi:10.3390/electronics8111351

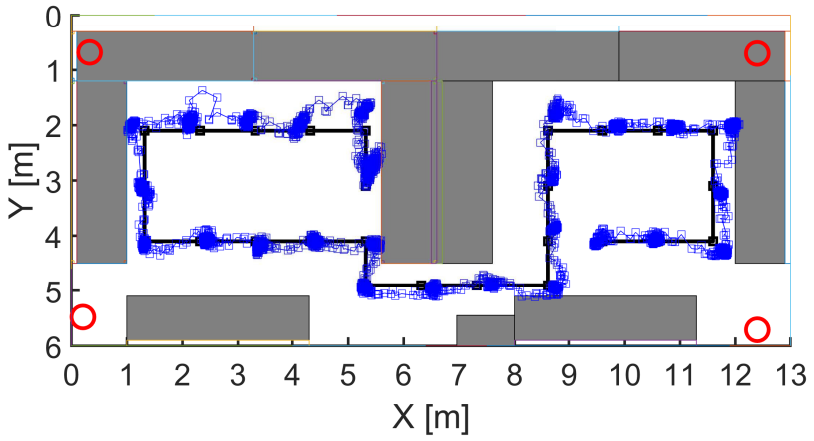

Figure 6. Estimation of the path for the fore-head position. The line with squares represents the ground-truth, and the continuous path with a cloud of points is the estimated path by the EKF.

always in LOS with the anchors. To better see the performance results, the main statistics are presented in the Table 5.

Table 5. Wearable positions with their localization error (in meters). P90 is the 90^{th} percentile.

Wearable Location	Mean	Median	P90	SD
Tripod	0.12	0.10	0.21	0.06
Fore-head	0.20	0.21	0.35	0.11
Hand	0.35	0.26	0.62	0.33
Ankle	0.50	0.36	0.97	0.36
Wrist	0.62	0.52	1.14	0.48
Thigh	0.68	0.57	1.46	0.45
Arm	1.36	1.26	2.47	0.77
Chest	2.46	2.55	4.04	1.66

Looking at Table 5, the first observation is the existence of a clear relationship between the localization performance and the body wearable sensor position. Overall, it can be observed that the fore-head and the chest position give the best [see – Fig. 7a] and worst [see – Fig. 7c] possible localization performance, respectively. In fact, in comparison with other the body wearable sensors, the errors obtained by the fore-head are closer to error obtained without the presence of the human body [see – tripod in Table 5]. In addition, 90 % of the estimates were below the error of 0.35 m and 4.04 m for the fore-head and chest, respectively. Similar to the ranging error, the reason for such a relatively good performance lies in the fact that the circular shape of the head allows the blocked signal to be diffracted to the wearable sensor in NLOS.

The performance of the chest is heavily influenced by NLOS conditions due to human body shadowing. Though all the wearable positions are influenced by human body shadowing effect, this effect is more pronounced at the chest. The large muscle size of the chest generates a big shadow zone, so the signal only reach the wearable sensor any reflections from nearby objects or walls in the surroundings. Therefore, the chest position can be used if it is possible to install enough anchors to minimize the risk of NLOS.

After the fore-head, the hand position obtains the second lowest errors as 90 % of the estimates were below the error of 0.62 m. The hand performs better than the chest though in both cases the

Preprints (www.preprints.org) | NOT PEER-REVIEWED | Posted: 23 September 2019 doi:10.20944/preprints201909.0266.v1

Peer-reviewed version available at Electronics 2019, 8, 1351; doi:10.3390/electronics8111351

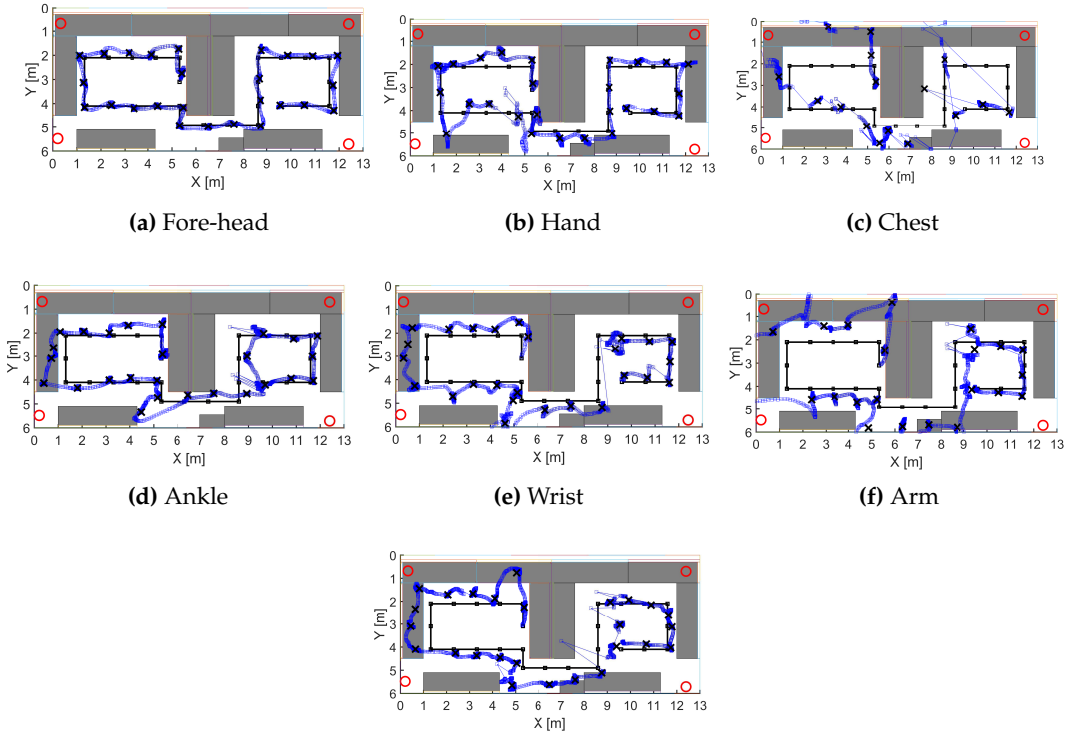

(a) Fore-head **(b)** Hand **(c)** Chest

(d) Ankle **(e)** Wrist **(f)** Arm

(g) Thigh

Figure 7. Estimation of the ground-truth positions after smoothing, filtering, and clustering. The marked crosses along the continuous path with clouds of points are the estimated ground-truth positions.

wearable is at the center of the chest because the space of 20 cm between the position of the hand and the chest [see – Fig. 3g] allows for creeping wave propagation during NLOS.

Among the wearable positions where the sensor is placed on side plane of the user, i.e., ankle, wrist, thigh and arm, the ankle gives the best performance as 90 % of the estimates were below the error of 0.97 m. Following the performance of the ankle position is the wrist, thigh, and arm locations with 90^{th} percentile of 1.14 m, 1.46 m, 2.47 m, respectively. Similar to the ranging performance, the differences in the position errors among these locations can be attributed to the differences in the thickness of the limb on which the sensor is attached.

7. Conclusion

We have presented a study of the effects of the body wearable sensor positions on UWB localization accuracy. The experiments have been performed with several LOS and NLOS conditions. While the positioning performance of forehead has been superior, the performance results for the chest position has been the lowest. Considering that multipath contributes localization errors of up to 0.2 m, the human body introduces errors of up to 0.14, 0.41, 0.76, 0.93, 1.25, 2.26, 3.83 m when the wearable is located at the fore-head, hand, ankle, wrist, thigh, arm, and chest, respectively

Future research will consider utilizing an appropriate body shadowing mitigation technique to minimise the errors created by the body.

Acknowledgments: The individual contributions of authors are specified as follows: Conceptualization, Timothy Otim and Peio Lopez-Iturri; methodology, Timothy Otim, Luis E. Díez, and Alfonso Bahillo; validation, Luis E. Díez, and Alfonso Bahillo; writing—original draft preparation, Timothy Otim; writing—review and editing,Timothy Otim, Luis E. Díez, Alfonso Bahillo, Peio Lopez-Iturri and Francisco Falcone; supervision, Alfonso Bahillo and Francisco Falcone.

Conflicts of Interest: The authors declare no conflict of interest.

Funding: This work was supported in part by the Research Training Grants Program of the University of Deusto, in part by REPNIN+ under Grant TEC2017-90808-REDT and in part by Ministerio de Ciencia, Innovación y Universidades, Gobierno de España under Grant RTI2018-095499-B-C31.

Reference

1. Harrop, P.; Hayward, J.; Das, R.; Holland, G. *Wearable Technology 2015-2025: Technologies, Markets, Forecast*; IDTechEx Research 2015.
2. Moayeri, N.; Mapar, J.; Tompkins, S.; Pahlavan, K. Emerging opportunities for localization and tracking [Guest Editorial]. *IEEE Wireless Communications* **2011**, *18*, 8–9. doi:10.1109/MWC.2011.5751290.
3. Mukhopadhyay, S.C. Wearable Sensors for Human Activity Monitoring: A Review. *IEEE Sensors Journal* **2015**, *15*, 1321–1330. doi:10.1109/JSEN.2014.2370945.
4. Lopez-Nava, I.H.; Munoz-Melendez, A. Wearable Inertial Sensors for Human Motion Analysis: A Review. *IEEE Sensors Journal* **2016**, *16*, 7821–7834. doi:10.1109/JSEN.2016.2609392.
5. Ramadhan, A. Wearable Smart System for Visually Impaired People. *Sensors* **2018**, *18*, 843. doi:10.3390/s18030843.
6. Puricer, P.; Kovar, P. Technical Limitations of GNSS Receivers in Indoor Positioning. 2007 17th International Conference Radioelektronika; IEEE: Brno, Czech Republic, 2007; pp. 1–5. doi:10.1109/RADIOELEK.2007.371487.
7. Ren, T.; Petovello, M.G. A Stand-Alone Approach for High-Sensitivity GNSS Receivers in Signal-Challenged Environment. *IEEE Transactions on Aerospace and Electronic Systems* **2017**, *53*, 2438–2448. doi:10.1109/TAES.2017.2699539.
8. Xu, R.; Chen, W.; Xu, Y.; Ji, S. A New Indoor Positioning System Architecture Using GPS Signals. *Sensors* **2015**, *15*, 10074–10087. doi:10.3390/s150510074.
9. Seco-Granados, G.; Lopez-Salcedo, J.; Jimenez-Banos, D.; Lopez-Risueno, G. Challenges in Indoor Global Navigation Satellite Systems: Unveiling its core features in signal processing. *IEEE Signal Processing Magazine* **2012**, *29*, 108–131. doi:10.1109/MSP.2011.943410.
10. Davidson, P.; Piche, R. A Survey of Selected Indoor Positioning Methods for Smartphones. *IEEE Communications Surveys & Tutorials* **2017**, *19*, 1347–1370. doi:10.1109/COMST.2016.2637663.
11. Jimenez Ruiz, A.R.; Seco Granja, F. Comparing Ubisense, BeSpoon, and DecaWave UWB Location Systems: Indoor Performance Analysis. *IEEE Transactions on Instrumentation and Measurement* **2017**, *66*, 2106–2117. doi:10.1109/TIM.2017.2681398.
12. Apple Invents iBeacon Version 2 using Ultra-Wide Band Radio Technology. https://www.patentlyapple.com/patently-apple/2019/01/apple-invents-ibeacon-version-2-using-ultra-wide-band-radio-technology.html. Accessed: 2019-09-04.
13. Lazzari, F.; Buffi, A.; Nepa, P.; Lazzari, S. Numerical Investigation of an UWB Localization Technique for Unmanned Aerial Vehicles in Outdoor Scenarios. *IEEE Sensors Journal* **2017**, *17*, 2896–2903. doi:10.1109/JSEN.2017.2684817.
14. Tiemann, J.; Schweikowski, F.; Wietfeld, C. Design of an UWB indoor-positioning system for UAV navigation in GNSS-denied environments. 2015 International Conference on Indoor Positioning and Indoor Navigation (IPIN); IEEE: Banff, AB, Canada, 2015; pp. 1–7. doi:10.1109/IPIN.2015.7346960.
15. Perakis, H.; Gikas, V. Evaluation of Range Error Calibration Models for Indoor UWB Positioning Applications. 2018 International Conference on Indoor Positioning and Indoor Navigation (IPIN); IEEE: Nantes, 2018; pp. 206–212. doi:10.1109/IPIN.2018.8533755.
16. Gengt, Y. Modeling the effect of human body on TOA ranging for indoor human tracking with wrist mounted sensor. *16th International Symposium on Wireless Personal Multimedia Communications (WPMC), Atlantic City, NJ*, **2013**, pp. 1–6.
17. He, J.; Geng, Y.; Pahlavan, K. Modeling indoor TOA ranging error for body mounted sensors. 2012 IEEE 23rd International Symposium on Personal, Indoor and Mobile Radio Communications - (PIMRC); IEEE: Sydney, Australia, 2012; pp. 682–686. doi:10.1109/PIMRC.2012.6362871.
18. Tian, Q.; Wang, K.I.K.; Salcic, Z. Human Body Shadowing Effect on UWB-Based Ranging System for Pedestrian Tracking. *IEEE Transactions on Instrumentation and Measurement* **2018**, pp. 1–10. doi:10.1109/TIM.2018.2884605.

19. Otim, T.; Bahillo, A.; Diez, L.E.; Lopez-Iturri, P.; Falcone, F. FDTD and Empirical Exploration of Human Body and UWB Radiation Interaction on TOF Ranging. *IEEE Antennas and Wireless Propagation Letters* **2019**, *18*, 1119–1123. doi:10.1109/LAWP.2019.2910378.
20. Otim, T.; Bahillo, A.; Diez, L.E.; Lopez-Iturri, P.; Falcone, F. Impact of Body Wearable Sensor Positions on UWB Ranging. *IEEE Sensors Journal* **2019**, pp. 1–1. doi:10.1109/JSEN.2019.2935634.
21. Vandrico Inc. Wearable Technology Database. http://vandrico.com/wearables/wearable-technology-database. Accessed: 2019-02-12.
22. Pourhomayoun, M.; Zhanpeng Jin.; Fowler, M.L. Accurate Localization of In-Body Medical Implants Based on Spatial Sparsity. *IEEE Transactions on Biomedical Engineering* **2014**, *61*, 590–597. doi:10.1109/TBME.2013.2284271.
23. Dove, I. Analysis of Radio Propagation Inside the Human Body for in-Body Localization Purposes. Master's thesis, University of Twente, 2014.
24. Christ, A.; Klingenbock, A.; Samaras, T.; Goiceanu, C.; Kuster, N. The dependence of electromagnetic far-field absorption on body tissue composition in the frequency range from 300 MHz to 6 GHz. *IEEE Transactions on Microwave Theory and Techniques* **2006**, *54*, 2188–2195. doi:10.1109/TMTT.2006.872789.
25. Kuster, N.; Santomaa, V.; Drossos, A. The dependence of electromagnetic energy absorption upon human head tissue composition in the frequency range of 300-3000 MHz. *IEEE Transactions on Microwave Theory and Techniques* **2000**, *48*, 1988–1995. doi:10.1109/22.884187.
26. Jiménez, A.R.; Seco, F. Comparing Decawave and Bespoon UWB location systems: indoor/outdoor performance analysis. Indoor Positioning and Indoor Navigation (IPIN), 2016 International Conference on. IEEE, 2016, pp. 1–8.
27. Zasowski, T.; Meyer, G.; Althaus, F.; Wittneben, A. UWB signal propagation at the human head. *IEEE Transactions on Microwave Theory and Techniques* **2006**, *54*, 1836–1845. doi:10.1109/TMTT.2006.871989.
28. Schmitt, S.; Adler, S.; Kyas, M. The effects of human body shadowing in RF-based indoor localization. Indoor Positioning and Indoor Navigation (IPIN), 2014 International Conference on. IEEE, 2014, pp. 307–313.
29. Bharadwaj, R.; Parini, C.; Alomainy, A. Experimental Investigation of 3-D Human Body Localization Using Wearable Ultra-Wideband Antennas. *IEEE Transactions on Antennas and Propagation* **2015**, *63*, 5035–5044. doi:10.1109/TAP.2015.2478455.
30. Diez, L.E.; Bahillo, A.; Otim, T.; Otegui, J. Step Length Estimation Using UWB Technology: A Preliminary Evaluation. 2018 International Conference on Indoor Positioning and Indoor Navigation (IPIN); IEEE: Nantes, 2018; pp. 1–8. doi:10.1109/IPIN.2018.8533731.
31. Ridolfi, M.; Vandermeeren, S.; Defraye, J.; Steendam, H.; Gerlo, J.; De Clercq, D.; Hoebeke, J.; De Poorter, E. Experimental Evaluation of UWB Indoor Positioning for Sport Postures. *Sensors* **2018**, *18*, 168. doi:10.3390/s18010168.

Sample Availability: Samples of the compounds ..... are available from the authors.